

# Nonlocal Patch-Based Fully Connected Tensor Network Decomposition for Multispectral Image Inpainting

Wen-Jie Zheng<sup>ID</sup>, Xi-Le Zhao<sup>ID</sup>, Yu-Bang Zheng<sup>ID</sup>, *Student Member, IEEE*, and Zhi-Feng Pang

**Abstract**—Multispectral image (MSI) inpainting plays an important role in real applications. Recently, fully connected tensor network (FCTN) decomposition has been shown the remarkable ability to fully characterize global correlation. Considering global correlation and nonlocal self-similarity (NSS) of MSIs, this letter introduces FCTN decomposition to the whole MSI and its NSS groups and proposes a novel nonlocal patch-based FCTN (NL-FCTN) decomposition for MSI inpainting. More specially, the NL-FCTN decomposition-based method, which increases tensor order by stacking similar small-sized patches to NSS groups, cleverly leverages the remarkable ability of FCTN decomposition to deal with higher-order tensors. Besides, we propose an efficient proximal alternating minimization (PAM)-based algorithm to solve the proposed NL-FCTN decomposition-based model with a theoretical convergence guarantee. Extensive experiments on MSIs demonstrate that the proposed method achieves the state-of-the-art inpainting performance among all compared methods.

**Index Terms**—Fully connected tensor network (FCTN) decomposition, multispectral image (MSI) inpainting, nonlocal self-similarity (NSS), tensor order increment.

## I. INTRODUCTION

MULTISPECTRAL images (MSIs) contain a wealth of spatial and spectral information, which makes them widely applied in various applications [1]–[3]. In practice, however, MSIs obtained are often incomplete due to some unavoidable factors, such as dead pixels and cloud cover. To improve subsequent practicability, it is important to estimate missing elements by MSI inpainting [4]–[6]. The core problem of MSI inpainting is to characterize the intrinsic prior of MSIs [7]–[11].

Global correlation is an important prior of MSIs. Since MSIs are usually modeled as higher-order tensors, whose

Manuscript received July 20, 2021; revised October 12, 2021; accepted October 29, 2021. Date of publication November 2, 2021; date of current version January 11, 2022. This work was supported in part by the National Natural Science Foundation of China under Grant 61876203 and Grant 12071345, in part by the Project for Applied Basic Research of Sichuan Province under Grant 2021YJ0107, and in part by the Program for Science and Technology Development of Henan Province under Grant 212102210511. (*Corresponding authors:* Xi-Le Zhao; Yu-Bang Zheng.)

Wen-Jie Zheng and Xi-Le Zhao are with the School of Mathematical Sciences, University of Electronic Science and Technology of China, Chengdu 611731, China (e-mail: wjz1355@163.com; xlzhao122003@163.com).

Yu-Bang Zheng is with the School of Mathematical Sciences, University of Electronic Science and Technology of China, Chengdu 611731, China, and also with the Tensor Learning Team, RIKEN Center for Advanced Intelligence Project, Tokyo 103-0027, Japan (e-mail: zhengyubang@163.com).

Zhi-Feng Pang is with the School of Mathematics and Statistics, Henan University, Kaifeng 475004, China (e-mail: zhifengpang@163.com).

Digital Object Identifier 10.1109/LGRS.2021.3124804

global correlation can be captured by tensor decomposition. There are various types of tensor decomposition, such as CANDECOMP/PARAFAC (CP) decomposition, Tucker decomposition, tensor singular value decomposition (t-SVD), tensor train (TT) decomposition, and tensor ring (TR) decomposition. All of them have been increasingly applied to MSI inpainting and achieved promising results. For example, Liu *et al.* [12] proposed a CP decomposition-based MSI denoising model, and Ng *et al.* [13] introduced a Tucker decomposition-based adaptive weighted sum of the nuclear norm (SNN) for MSI inpainting. Based on t-SVD, Fan *et al.* [14] used tensor nuclear norm (TNN) to MSI inpainting, and Zheng *et al.* [15] further expanded TNN to convex three-directional TNN and non-convex three-directional log-based TNN and proposed two models for mixed noise removal. TT and TR decompositions, two representative tensor network decompositions, received extensive applications in image restoration, since they have the superior capability to deal with higher-order tensors. For example, Bengua *et al.* [16] first proposed a TT decomposition-based image inpainting model, and Ding *et al.* [17] further embedded a total variation (TV) regularization into TT decomposition to improve the capability of image details recovery. Based on TR decomposition, Yuan *et al.* [18] and He *et al.* [19] proposed an image inpainting method by combining factor regularization and TV regularization, respectively.

However, the above methods directly considered global correlation, which ignored the redundancy of repeated local patches across the spatial modes of MSIs, i.e., nonlocal self-similarity (NSS). One way to fully use NSS prior is to apply tensor low-rank method, such as log-based SNN [20] and TNN, to each NSS group [21], which is a new tensor obtained by stacking similar small-sized patches. By taking a third-order MSI as an example, each original NSS group is a fourth-order tensor, including two spatial modes, one spectral mode, and one similar-group mode. However, traditional methods usually reshaped two spatial modes in each NSS group to one mode, which cannot better preserve the spatial structure of each NSS group. Therefore, Ding *et al.* [22] exploited TT rank minimization to the original fourth-order NSS groups and achieved promising completion results. But TT decomposition only characterizes the correlation between adjacent two modes, causing a limited characterization for the NSS groups.

Recently, a fully connected tensor network (FCTN) decomposition has been proposed, which establishes an operation between any two modes and has the powerful capability to capture global correlation of tensors [23]. Based on FCTN decomposition, this letter makes twofold contribution listing as follows.

1558-0571 © 2021 IEEE. Personal use is permitted, but republication/redistribution requires IEEE permission.  
See <https://www.ieee.org/publications/rights/index.html> for more information.

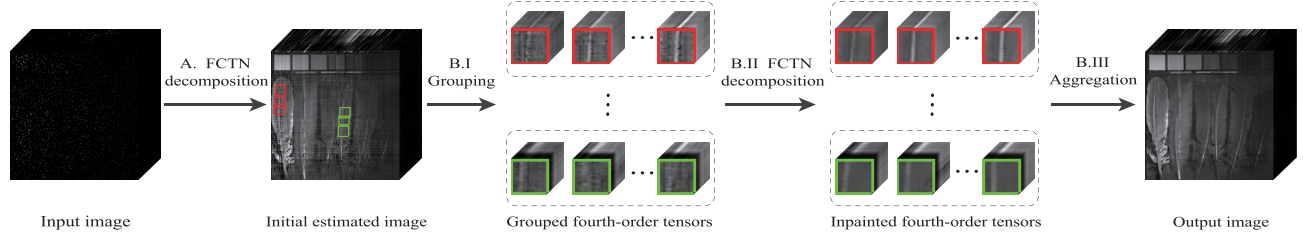


Fig. 1. Flowchart of the proposed MSI inpainting method. It involves two stages: A. initial FCTN decomposition inpainting and B. NL-FCTN decomposition inpainting. B includes three steps consisting of grouping, grouped FCTN decomposition inpainting, and aggregation.

TABLE I  
NOTATION DECLARATIONS

Notations	Interpretations
$x, \mathbf{x}, \mathbf{X}, \mathcal{X}$	scalar, vector, matrix, tensor
$\mathcal{X}(i_1, i_2, \dots, i_N)$	the $(i_1, i_2, \dots, i_N)$ th element of $\mathcal{X}$
$\mathcal{X}_{1:d}$	$(\mathcal{X}_1, \mathcal{X}_2, \dots, \mathcal{X}_d)$
$\ \mathcal{X}\ _F$	$\ \mathcal{X}\ _F = \sqrt{\sum_{i_1, i_2, \dots, i_N}  \mathcal{X}(i_1, i_2, \dots, i_N) ^2}$

First, we suggest a novel nonlocal patch-based FCTN (NL-FCTN) decomposition-based MSI inpainting model, the flowchart of which is illustrated in Fig 1. As shown in Fig 1, the proposed model has two advantages. On one hand, using FCTN decomposition to the whole MSI and its NSS groups fully captures global correlation and NSS of MSIs. On the other hand, NL-FCTN decomposition-based method regards the process of stacking similar small-sized patches to NSS groups as a tensor order increment operation, which cleverly leverages the remarkable ability of FCTN decomposition for characterizing higher-order tensors.

Second, we develop a proximal alternating minimization (PAM)-based algorithm to solve the NL-FCTN decomposition-based model with a theoretical guarantee of convergence. Extensive experiments show that the proposed method outperforms the state-of-the-art methods on MSI inpainting.

## II. NOTATIONS

We summarize the notations throughout this letter in Table I and introduce a generalized tensor unfolding operation following [23]. Supposing that  $\mathbf{n}$  is a reordering of the vector  $(1, 2, \dots, N)$ , the generalized tensor unfolding represents an  $N$ th-order tensor  $\mathcal{X} \in \mathbb{R}^{I_1 \times I_2 \times \dots \times I_N}$  as a matrix  $\mathbf{X} \in \mathbb{R}^{\prod_{i=1}^d I_{n_i} \times \prod_{i=d+1}^N I_{n_i}}$ , which is denoted by  $\mathbf{X}_{[n_{1:d}; n_{d+1:N}]} = \text{GenUnfold}(\mathcal{X}, n_{1:d}; n_{d+1:N})$ . On the contrary, its inverse operation is denoted by  $\mathcal{X} = \text{GenFold}(\mathbf{X}_{[n_{1:d}; n_{d+1:N}]}, n_{1:d}; n_{d+1:N})$ . Especially, we simply denote  $\mathbf{X}_{[i; 1, 2, \dots, i-1, i+1, \dots, N]}$  by  $\mathbf{X}_{(i)}$  and let  $\mathcal{X} = \text{Fold}(\mathbf{X}_{(i)})$ .

## III. PROPOSED MSI INPAINTING METHOD

In this section, we start with a brief introduction to the definition and properties of FCTN decomposition and then introduce the proposed NL-FCTN decomposition-based method for MSI inpainting in detail.

### A. FCTN Decomposition

Compared with TT and TR decompositions, FCTN decomposition is more efficient and more general. Specifically, by factorizing an  $N$ th-order tensor into a sequence of small-sized  $N$ th-order factor tensors and establishing the relationship between any two factors, FCTN decomposition has the

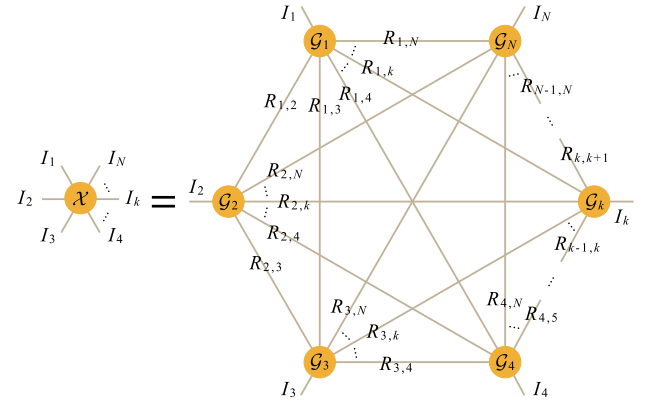


Fig. 2. Illustration of FCTN decomposition.

remarkable ability to fully characterize global correlation of tensors. Mathematically, given an  $N$ th-order tensor  $\mathcal{X} \in \mathbb{R}^{I_1 \times I_2 \times \dots \times I_N}$ , FCTN decomposition denotes each element of  $\mathcal{X}$  by

$$\begin{aligned} & \mathcal{X}(i_1, i_2, \dots, i_N) \\ &= \sum_{r_{1,2}=1}^{R_{1,2}} \sum_{r_{1,3}=1}^{R_{1,3}}, \dots, \sum_{r_{1,N}=1}^{R_{1,N}} \sum_{r_{2,3}=1}^{R_{2,3}}, \dots, \sum_{r_{2,N}=1}^{R_{2,N}}, \dots, \sum_{r_{N-1,N}=1}^{R_{N-1,N}} \\ & \quad \{ \mathcal{G}_1(i_1, r_{1,2}, r_{1,3}, \dots, r_{1,N}) \\ & \quad \times \mathcal{G}_2(r_{1,2}, i_2, r_{2,3}, \dots, r_{2,N}) \times \dots \\ & \quad \times \mathcal{G}_k(r_{1,k}, r_{2,k}, \dots, r_{k-1,k}, i_k, r_{k,k+1}, \dots, r_{k,N}) \times \dots \\ & \quad \times \mathcal{G}_N(r_{1,N}, r_{2,N}, \dots, r_{N-1,N}, i_N) \} \end{aligned} \quad (1)$$

where  $\mathcal{G}_k \in \mathbb{R}^{R_{1,k} \times R_{2,k} \times \dots \times R_{k-1,k} \times I_k \times R_{k,k+1} \times \dots \times R_{k,N}}$  ( $k = 1, 2, \dots, N$ ) are called the FCTN factors and the vector  $(R_{1,2}, R_{1,3}, \dots, R_{1,N}, R_{2,3}, \dots, R_{2,N}, \dots, R_{N-1,N})$  is called the FCTN rank. For the sake of simplicity, (1) can be expressed as  $\mathcal{X} = \text{FCTN}(\mathcal{G}_1, \mathcal{G}_2, \dots, \mathcal{G}_N)$ .

Fig. 2 vividly illustrates the graphic structure of FCTN decomposition. In Fig. 2, we can clearly observe that any two FCTN factors are linked by a line, representing a multi-linear operation, i.e., tensor contraction [23], between them.

### B. NL-FCTN Decomposition-Based MSI Inpainting Method

The following is a detailed derivation of the proposed NL-FCTN decomposition-based model for MSI inpainting with the Fig. 1. The model consists of two stages. In stage A, we use FCTN decomposition to the whole MSI as an initialization process, which not only uses global correlation of whole MSI but also guarantees high accuracy of subsequent group matching.

In stage B, there are three steps. In step B.I, we divide the initial MSI into small-sized patches and stack similar

**Algorithm 1** PAM-Based Algorithm for NL-FCTN Decomposition-Based MSI Inpainting Model

**Input:** The degraded MSI  $\mathcal{T} \in \mathbb{R}^{I_1 \times I_2 \times \dots \times I_N}$ , the index set  $\Omega$ , the patch size  $p$ , the similar patch number  $s$ , and the FCTN-rank  $R$  of each NSS groups.

**Initialization:** The initial iterations  $q = 0$ , the maximum iterations  $q_{\max} = 100$ , and  $\rho = 0.01$ .

1: **Stage A. initial FCTN decomposition inpainting**

2: Inpaint the degraded MSI  $\mathcal{T}$  via FCTN decomposition and obtain an initial MSI  $\mathcal{F}$ .

3: **Stage B. nonlocal FCTN decomposition inpainting**

4: (I) Group similar patches over all bands of  $\mathcal{F}$  and obtain a set of  $(N+1)$ th-order NSS groups  $\{\hat{\mathcal{F}}_l\}_{l=1}^L$ .

5: (II) Inpaint each NSS group  $\hat{\mathcal{F}}_l$  via FCTN decomposition

6: **for**  $l = 1 : L$  **do**

7:   **for**  $q = 1 : q_{\max}$  **do**

8:     Update  $\mathcal{G}_{l,i}^{(q+1)}$  via (5).

9:     Update  $\hat{\mathcal{X}}_l^{(q+1)}$  via (5).

10:   **end for**

11: **end for**

12: (III) Aggregate the inpainted NSS groups  $\{\hat{\mathcal{X}}_l\}_{l=1}^L$  to form the inpainted MSI  $\mathcal{X}$ .

**Output:** The inpainted MSI  $\mathcal{X}$ .

patches as NSS groups. By taking an MSI  $\mathcal{F} \in \mathbb{R}^{I_1 \times I_2 \times I_3}$  as an example, we divide it into overlapped cubes  $\{\mathcal{F}_t \in \mathbb{R}^{p \times p \times I_3}\}_{t=1}^T$  with patch size  $p$  and row/column stride 1, where  $T = ((I_1 - p + 1) \times ((I_2 - p + 1))$  is the number of total patches. Similarly, we obtain key patches from  $\mathcal{F}$  by setting row/column stride to  $p - 1$  and the number of key patches is  $L = ((I_1 - p)/(p - 1) + 1) \times ((I_2 - p)/(p - 1) + 1)$ . The way to obtain each NSS group is to use the Euclidean distance to access similarity between each key patch and all total patches and cluster the first  $s$  similar patches. The NSS groups of MSI are denoted by  $\{\hat{\mathcal{F}}_l \in \mathbb{R}^{p \times p \times I_3 \times s}\}_{l=1}^L$ . Thus, a third-order MSI  $\mathcal{F}$  transforms into a set of fourth-order NSS groups  $\{\hat{\mathcal{F}}_l\}_{l=1}^L$  by group matching. Following a similar step described above, a fourth-order time-series MSI with the size of  $I_1 \times I_2 \times I_3 \times I_4$  transforms into a set of fifth-order NSS groups with the size of  $p \times p \times I_3 \times I_4 \times s$ . More generally, an  $N$ th-order tensor naturally transforms into a set of  $(N+1)$ th-order NSS groups.

In step B.II, we regard an NSS group as a basis inpainting unit because of its strong global correlation and introduce FCTN decomposition to each NSS group. For FCTN decomposition, this step not only makes full use of the remarkable ability to characterize global correlation but also cleverly leverages the advantage of dealing with higher-order tensors by NSS-based tensor order increment operation.

Without loss of generality, we consider an  $(N+1)$ th-order NSS group  $\hat{\mathcal{F}}_l$  and use FCTN decomposition to obtain the inpainted NSS group  $\hat{\mathcal{X}}_l$ , which can be formulated as

$$\begin{aligned} & \min_{\hat{\mathcal{X}}_l, \mathcal{G}_l} \frac{1}{2} \left\| \hat{\mathcal{X}}_l - \text{FCTN}(\mathcal{G}_{l,1}, \mathcal{G}_{l,2}, \dots, \mathcal{G}_{l,N+1}) \right\|_F^2 \\ & \text{s.t. } \mathcal{P}_{\Omega_l}(\hat{\mathcal{X}}_l) = \mathcal{P}_{\Omega_l}(\hat{\mathcal{F}}_l) \end{aligned} \quad (2)$$

where  $\mathcal{P}_{\Omega_l}(\cdot)$  is the projection operator that maps the entries in  $\Omega_l$  to themselves and others to zero, and  $\Omega_l$  is the index of

known elements in  $\hat{\mathcal{F}}_l$ . Since (2) is convex for  $\hat{\mathcal{X}}_l$  and its FCTN factors  $\mathcal{G}_{l,i}$  ( $i = 1, 2, \dots, N+1$ ) independently, PAM [24] is introduced to obtain the solution as follows:

$$\begin{cases} \mathcal{G}_{l,i}^{(q+1)} = \underset{\mathcal{G}_{l,i}}{\operatorname{argmin}} \left\{ \frac{1}{2} \left\| \hat{\mathcal{X}}_l^{(q)} - \text{FCTN}(\mathcal{G}_{l,1:i-1}^{(q+1)}, \mathcal{G}_{l,i}, \mathcal{G}_{l,i+1:N+1}^{(q)}) \right\|_F^2 \right. \\ \quad \left. + \frac{\rho}{2} \left\| \mathcal{G}_{l,i} - \mathcal{G}_{l,i}^{(q)} \right\|_F^2 \right\} \\ \quad i = 1, 2, \dots, N+1 \\ \hat{\mathcal{X}}_l^{(q+1)} = \underset{\mathcal{P}_{\Omega_l}(\hat{\mathcal{X}}_l) = \mathcal{P}_{\Omega_l}(\hat{\mathcal{F}}_l)}{\operatorname{argmin}} \left\{ \frac{1}{2} \left\| \hat{\mathcal{X}}_l - \text{FCTN}(\mathcal{G}_{l,1:N+1}^{(q+1)}) \right\|_F^2 \right. \\ \quad \left. + \frac{\rho}{2} \left\| \hat{\mathcal{X}}_l - \hat{\mathcal{X}}_l^{(q)} \right\|_F^2 \right\} \end{cases} \quad (3)$$

where  $\mathcal{G}_{l,i}^{(q)}$  and  $\hat{\mathcal{X}}_l^{(q)}$  are the results of the  $q$ th iteration of  $\mathcal{G}_{l,i}$  and  $\hat{\mathcal{X}}_l$ , respectively, and  $\rho > 0$  is a proximal parameter. According to Theorem 4 in [23]

$$\hat{\mathbf{X}}_{l(i)} = (\mathbf{G}_{l,i})_{(i)} (\mathbf{M}_{l,i})_{[m_{1:N}; n_{1:N}]}$$

where  $\mathcal{M}_{l,i} = \text{FCTN}(\{\mathcal{G}_{l,i}\}_{i=1}^{N+1}, / \mathcal{G}_{l,i})$  is a composition of  $\mathcal{G}_{l,1}, \mathcal{G}_{l,2}, \dots, \mathcal{G}_{l,i-1}, \mathcal{G}_{l,i+1}, \dots, \mathcal{G}_{l,N+1}$

$$m_j = \begin{cases} 2j, & \text{if } j < i \\ 2j-1, & \text{if } j \geq i \end{cases} \quad \text{and} \quad n_j = \begin{cases} 2j-1, & \text{if } j < i \\ 2j, & \text{if } j \geq i. \end{cases}$$

Thus, the  $\mathcal{G}_{l,i}$  ( $i = 1, 2, \dots, N+1$ )-subproblems are given by

$$\begin{aligned} \mathcal{G}_{l,i}^{(q+1)} &= \underset{\mathcal{G}_{l,i}}{\operatorname{argmin}} \left\{ \frac{\rho}{2} \left\| \mathcal{G}_{l,i} - \mathcal{G}_{l,i}^{(q)} \right\|_F^2 \right. \\ &\quad \left. + \frac{1}{2} \left\| \hat{\mathbf{X}}_{l(i)}^{(q)} - (\mathbf{G}_{l,i})_{(i)} (\mathbf{M}_{l,i}^{(q)})_{[m_{1:N}; n_{1:N}]} \right\|_F^2 \right\}. \end{aligned} \quad (4)$$

It is easy to find that (3) and (4) have the closed-form solutions as

$$\begin{cases} \mathcal{G}_{l,i}^{(q+1)} = \text{FOLD} \\ \quad \left( \hat{\mathbf{X}}_{l(i)}^{(q)} (\mathbf{M}_{l,i}^{(q)})_{[n_{1:N}; m_{1:N}]} + \rho (\mathbf{G}_{l,i}^{(q)})_{(i)} \right) \\ \quad \times \left[ (\mathbf{M}_{l,i}^{(q)})_{[m_{1:N}; n_{1:N}]} (\mathbf{M}_{l,i}^{(q)})_{[n_{1:N}; m_{1:N}]} + \rho \mathbf{I} \right]^{-1} \\ \quad i = 1, 2, \dots, N+1 \\ \hat{\mathcal{X}}_l^{(q+1)} = \mathcal{P}_{\Omega_l} \left( \frac{\text{FCTN}(\{\mathcal{G}_{l,i}^{(q+1)}\}_{i=1}^{N+1}) + \rho \hat{\mathcal{X}}_l^{(q)}}{1 + \rho} \right) \\ \quad + \mathcal{P}_{\Omega_l}(\hat{\mathcal{F}}_l). \end{cases} \quad (5)$$

In step B.III, we aggregate the inpainted NSS groups  $\{\hat{\mathcal{X}}_l\}_{l=1}^L$  to their original positions and obtain the whole inpainted MSI  $\mathcal{X}$ .

The above NL-FCTN decomposition-based method for MSI inpainting is summarized in Algorithm 1. Its theoretical convergence can be similarly proved following [23].

TABLE II  
AVERAGE PSNR, SSIM, SAM, AND RUNNING TIME OF 32 TESTING MSIs OBTAINED BY DIFFERENT COMPARED METHODS

MR	98%				95%				90%				80%			
	PSNR	SSIM	SAM	Time (s)	PSNR	SSIM	SAM	Time (s)	PSNR	SSIM	SAM	Time (s)	PSNR	SSIM	SAM	Time (s)
KBR-TC	22.640	0.642	20.400	150.89	33.548	0.911	6.809	151.05	41.729	0.977	3.446	155.14	48.536	0.994	1.972	162.95
NL-SNN	16.570	0.642	17.900	1985.5	29.648	0.864	6.111	2032.6	41.303	0.977	2.537	2044.3	47.365	0.991	1.712	2048.3
NL-TNN	19.822	0.656	26.313	69.608	31.698	0.921	8.629	70.766	36.773	0.970	3.947	71.294	44.186	0.993	1.761	72.850
NL-TT	26.371	0.786	15.267	301.30	31.486	0.905	6.680	305.40	34.736	0.947	3.914	306.17	38.426	0.975	2.516	309.41
FCTN-TC	25.994	0.662	19.188	36.168	33.022	0.863	9.832	55.352	37.726	0.937	6.673	91.170	43.682	0.976	4.212	155.88
NL-FCTN	<b>28.494</b>	<b>0.804</b>	<b>11.952</b>	542.20	<b>37.537</b>	<b>0.959</b>	<b>3.985</b>	544.17	<b>44.286</b>	<b>0.990</b>	<b>2.070</b>	542.31	<b>49.717</b>	<b>0.996</b>	<b>1.336</b>	542.38

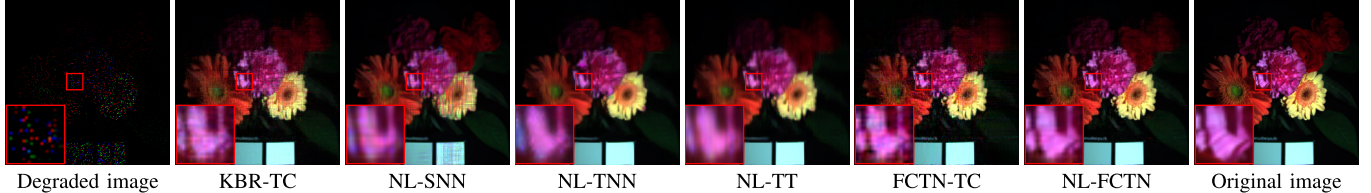


Fig. 3. Restoration results of *flowers* with MR = 95%. The pseudo color images are composed of bands 29, 14, and 5.

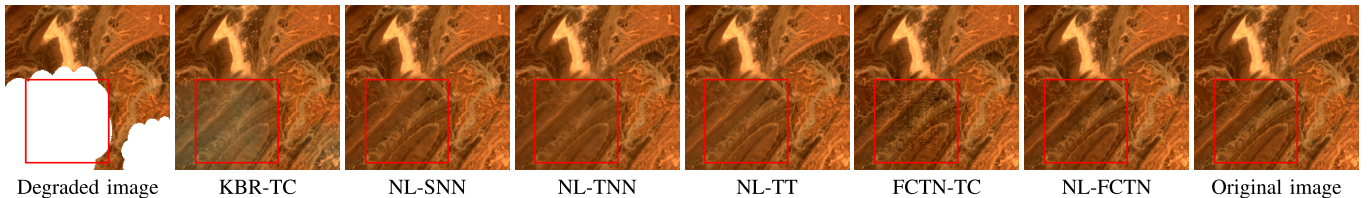


Fig. 4. Simulated cloud removal results of *Morocco*. The pseudo color images are composed of bands 3, 2, and 1 at the second time node.

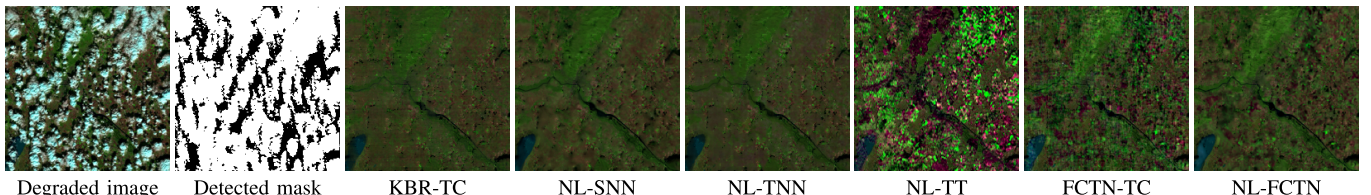


Fig. 5. Real cloud removal results of *Bratislava*. The pseudo color images are composed of bands 5, 3, and 1 at the fifth time node.

#### IV. NUMERICAL EXPERIMENTS

In this section, we test the performance of NL-FCTN decomposition-based method for MSI inpainting on 32 MSIs (third-order tensors) and two time-series MSIs (fourth-order tensors). The compared methods are global tensor decomposition-based tensor completion (TC) methods including KBR-TC [25] and FCTN-TC [23], and nonlocal patch-based tensor decomposition for TC including NL-SNN [20], NL-TNN [21], and NL-TT [22]. All hyper-parameters of each compared method are set for optimal performance according to the authors' paper and code. Three evaluation indexes contain the peak signal-to-noise rate (PSNR), structural similarity (SSIM), and spectral angle mapping (SAM). Here, the PSNR and SSIM values are obtained by averaging the values of PSNR and SSIM of all bands. The SAM values are obtained by averaging the values of SAM of all spectral vectors.

1) *MSI Inpainting*: We test the CAVE Database<sup>1</sup> with 32 MSIs. Each test MSI is resized to 256 × 256 × 31. The missing rate (MR) is defined as the rate of the unknown elements in the total elements. We test four MRs: 98%, 95%, 90%, and 80%. Table II reports the average values of PSNR, SSIM, SAM, and running time of all 32 MSIs obtained by

all compared methods under each MR. We observe that the proposed method performs better than the compared methods for PSNR, SSIM, and SAM, while costing moderate running times. This is because NL-FCTN introduces FCTN-TC to the whole MSI and its NSS groups, which boosts the performance of FCTN decomposition on higher-order tensors.

Fig. 3 shows the pseudo color images of restoration results with MR = 95% of *flowers*. As observed, the proposed method achieves superior inpainting results visually. In particular, the spatial textures of MSIs can be better preserved, such as the *flowers*.

2) *Time-Series MSI Cloud Removal*: We test two datasets of the time-series sentinel-2 images. *Morocco*<sup>2</sup> is taken over Morocco, which is resized to 200 × 200 × 4 × 6. To simulate the cloud mask of real scene on *Morocco*, we set that: 1) at different time nodes, the clouds are located at different locations and 2) at the same time node, the clouds are located at the same location in all bands. *Bratislava*<sup>3</sup> is taken over Bratislava with a real cloud mask detected by multi-scale convolutional feature fusion [26], which is resized to 200 × 200 × 6 × 7. Table III reports the PSNR, SSIM, SAM, and running time on the cloud removal results of

<sup>1</sup><https://www.cs.columbia.edu/CAVE/databases/multispectral/>

<sup>2</sup><https://theia.cnes.fr/atdistrib/rocket/#/home>

<sup>3</sup><https://earthexplorer.usgs.gov>

TABLE III  
PSNR, SSIM, SAM, AND RUNNING TIME OF MOROCCO  
OBTAINED BY DIFFERENT COMPARED METHODS

Method	PSNR	SSIM	SAM	Time (s)
KBR-TC	33.853	0.970	2.745	100.21
NL-SNN	46.891	0.988	0.336	63.553
NL-TNN	43.089	0.981	0.446	341.81
NL-TT	39.777	0.907	1.249	190.23
FCTN-TC	44.128	0.982	0.363	240.69
NL-FCTN	<b>48.132</b>	<b>0.994</b>	<b>0.243</b>	686.86

*Morocco* obtained by all compared methods. We observe that the proposed method achieves outstanding results regardless of RSNR, SSIM, or SAM within an acceptable time.

Fig. 4 shows the pseudo images of the simulated cloud removal results of *Morocco* at the second time node. Especially in the red box, we observe that KBR-TC cannot better preserve the spectral information and causes color loss; NL-SNN, NL-TNN, and NL-TT blur the detail textures of the spatial images; FCTN-TC preserves the details but causes some artifacts; NL-FCTN achieves the closest result to the original images among all compared methods. Fig. 5 displays the pseudo images of the real cloud removal results of *Bratislava* at the fifth time node. As observed, the results obtained by KBR-TC, NL-SNN, and NL-TNN are over-smoothed and lose local details, and the results obtained by NL-TT and FCTN-TC contain artifacts. On the contrary, NL-FCTN obtains the best visual result, both in global structure recovery and local details preserving.

## V. CONCLUSION

In this letter, we proposed an NL-FCTN decomposition-based method for MSI inpainting. We introduced FCTN decomposition to the whole MSI and its NSS groups to fully characterize global correlation and NSS of MSIs. From another perspective, we combined FCTN decomposition with the nonlocal patch-based tensor order increment operation, which cleverly leverages its remarkable ability on higher-order tensors. The NL-FCTN decomposition-based model was solved by a PAM-based algorithm with a theoretical convergence guarantee. Extensive experiments proved that the proposed method performed better than all compared methods.

## REFERENCES

- [1] W. Sun, G. Yang, J. Peng, and Q. Du, "Lateral-slice sparse tensor robust principal component analysis for hyperspectral image classification," *IEEE Geosci. Remote Sens. Lett.*, vol. 17, no. 1, pp. 107–111, Jan. 2020.
- [2] Y. Chen, W. He, N. Yokoya, T.-Z. Huang, and X.-L. Zhao, "Nonlocal tensor-ring decomposition for hyperspectral image denoising," *IEEE Trans. Geosci. Remote Sens.*, vol. 58, no. 2, pp. 1348–1362, Oct. 2019.
- [3] D. Hong *et al.*, "Interpretable hyperspectral artificial intelligence: When nonconvex modeling meets hyperspectral remote sensing," *IEEE Geosci. Remote Sens. Mag.*, vol. 9, no. 2, pp. 52–87, Jun. 2021.
- [4] M. Wang, Q. Wang, J. Chanussot, and D. Hong, "Total variation regularized weighted tensor ring decomposition for missing data recovery in high-dimensional optical remote sensing images," *IEEE Geosci. Remote Sens. Lett.*, early access, Apr. 9, 2021, doi: [10.1109/LGRS.2021.3069895](https://doi.org/10.1109/LGRS.2021.3069895).
- [5] Q. Yuan, Q. Zhang, J. Li, H. Shen, and L. Zhang, "Hyperspectral image denoising employing a spatial–spectral deep residual convolutional neural network," *IEEE Trans. Geosci. Remote Sens.*, vol. 57, no. 2, pp. 1205–1218, Feb. 2018.
- [6] R. Dian and S. Li, "Hyperspectral image super-resolution via subspace-based low tensor multi-rank regularization," *IEEE Trans. Image Process.*, vol. 28, no. 10, pp. 5135–5146, Oct. 2019.
- [7] W. He *et al.*, "Non-local meets global: An integrated paradigm for hyperspectral image restoration," *IEEE Trans. Pattern Anal. Mach. Intell.*, early access, Sep. 29, 2020, doi: [10.1109/TPAMI.2020.3027563](https://doi.org/10.1109/TPAMI.2020.3027563).
- [8] Q. Zhang, Q. Yuan, J. Li, X. Liu, H. Shen, and L. Zhang, "Hybrid noise removal in hyperspectral imagery with a spatial–spectral gradient network," *IEEE Trans. Geosci. Remote Sens.*, vol. 57, no. 10, pp. 7317–7329, Dec. 2019.
- [9] L. Zhuang, L. Gao, B. Zhang, X. Fu, and J. M. Bioucas-Dias, "Hyperspectral image denoising and anomaly detection based on low-rank and sparse representations," *IEEE Trans. Geosci. Remote Sens.*, early access, Dec. 9, 2021, doi: [10.1109/TGRS.2020.3040221](https://doi.org/10.1109/TGRS.2020.3040221).
- [10] L. Zhuang, X. Fu, M. K. Ng, and J. M. Bioucas-Dias, "Hyperspectral image denoising based on global and nonlocal low-rank factorizations," *IEEE Trans. Geosci. Remote Sens.*, early access, Jan. 8, 2021, doi: [10.1109/TGRS.2020.3046038](https://doi.org/10.1109/TGRS.2020.3046038).
- [11] H. Zhang, L. Liu, W. He, and L. Zhang, "Hyperspectral image denoising with total variation regularization and nonlocal low-rank tensor decomposition," *IEEE Trans. Geosci. Remote Sens.*, vol. 58, no. 5, pp. 3071–3084, May 2019.
- [12] X. Liu, S. Bourennane, and C. Fossati, "Denoising of hyperspectral images using the PARAFAC model and statistical performance analysis," *IEEE Trans. Geosci. Remote Sens.*, vol. 50, no. 10, pp. 3717–3724, Oct. 2012.
- [13] M. K.-P. Ng, Q. Yuan, L. Yan, and J. Sun, "An adaptive weighted tensor completion method for the recovery of remote sensing images with missing data," *IEEE Trans. Geosci. Remote Sens.*, vol. 55, no. 6, pp. 3367–3381, Jun. 2017.
- [14] H. Fan, Y. Chen, Y. Guo, H. Zhang, and G. Kuang, "Hyperspectral image restoration using low-rank tensor recovery," *IEEE J. Sel. Topics Appl. Earth Observ., Remote Sens.*, vol. 10, no. 10, pp. 4589–4604, Oct. 2017.
- [15] Y.-B. Zheng, T.-Z. Huang, X.-L. Zhao, T.-X. Jiang, T.-H. Ma, and T.-Y. Ji, "Mixed noise removal in hyperspectral image via low-fibered-rank regularization," *IEEE Trans. Geosci. Remote Sens.*, vol. 58, no. 1, pp. 734–749, Jan. 2020.
- [16] J. A. Bengua, H. N. Phien, H. D. Tuan, and M. N. Do, "Efficient tensor completion for color image and video recovery: Low-rank tensor train," *IEEE Trans. Image Process.*, vol. 26, no. 5, pp. 2466–2479, May 2017.
- [17] M. Ding, T.-Z. Huang, T.-Y. Ji, X.-L. Zhao, and J.-H. Yang, "Low-rank tensor completion using matrix factorization based on tensor train rank and total variation," *J. Sci. Comput.*, vol. 81, no. 2, pp. 941–964, Nov. 2019.
- [18] L. Yuan, C. Li, D. Mandic, J. Cao, and Q. Zhao, "Tensor ring decomposition with rank minimization on latent space: An efficient approach for tensor completion," in *Proc. AAAI*, 2019, vol. 33, no. 1, pp. 9151–9158.
- [19] W. He, N. Yokoya, L. Yuan, and Q. Zhao, "Remote sensing image reconstruction using tensor ring completion and total variation," *IEEE Trans. Geosci. Remote Sens.*, vol. 57, no. 11, pp. 8998–9009, Nov. 2019.
- [20] T. Xie, S. Li, L. Fang, and L. Liu, "Tensor completion via non-local low-rank regularization," *IEEE Trans. Cybern.*, vol. 49, no. 6, pp. 2344–2354, Jun. 2019.
- [21] L. Song, B. Du, L. Zhang, L. Zhang, J. Wu, and X. Li, "Nonlocal patch based t-SVD for image inpainting: Algorithm and error analysis," in *Proc. AAAI*, 2018, vol. 32, no. 1, pp. 2419–2426.
- [22] M. Ding, T.-Z. Huang, X.-L. Zhao, M. K. Ng, and T.-H. Ma, "Tensor train rank minimization with nonlocal self-similarity for tensor completion," *Inverse Problem Imag.*, vol. 15, no. 3, pp. 475–498, 2021.
- [23] Y.-B. Zheng, T.-Z. Huang, X.-L. Zhao, Q. Zhao, and T.-X. Jiang, "Fully-connected tensor network decomposition and its application to higher-order tensor completion," in *Proc. AAAI*, 2021, vol. 35, no. 12, pp. 11071–11078.
- [24] H. Attouch, J. Bolte, and B. F. Svaiter, "Convergence of descent methods for semi-algebraic and tame problems: Proximal algorithms, forward–backward splitting, and regularized Gauss–Seidel methods," *Math. Program.*, vol. 137, nos. 1–2, pp. 91–129, 2013.
- [25] Q. Xie, Q. Zhao, D. Meng, and Z. Xu, "Kronecker-basis-representation based tensor sparsity and its applications to tensor recovery," *IEEE Trans. Pattern Anal. Mach. Intell.*, vol. 40, no. 8, pp. 1888–1902, Aug. 2018.
- [26] Z. Li, H. Shen, Q. Cheng, Y. Liu, S. You, and Z. He, "Deep learning based cloud detection for medium and high resolution remote sensing images of different sensors," *ISPRS J. Photogramm. Remote Sens.*, vol. 150, pp. 197–212, Apr. 2019.